Int. J. Heat Mass Transfer. Vol. 34, No. 9, pp. 2265–2273, 1991
Printed in Great Britain

0017–9310/91 $3.00 + 0.00

Analysis of combined conductive and radiative heat transfer in a two-dimensional rectangular enclosure using the discrete ordinates method

TAIK YOUNG KIM and SEUNG WOOK BAEK
Korea Advanced Institute of Science and Technology,
Aerospace Engineering Department, P.O. Box 150, Cheongryang, Seoul, Korea

(*Received* 29 *June* 1990 *and in final form* 27 *September* 1990)

Abstract—An efficient tool to deal with multidimensional radiative heat transfer is in strong demand to analyse the various thermal problems combined either with other modes of heat transfer or with combustion phenomena. The current study examines the discrete ordinates method (DOM) for coupled radiative and conductive heat transfer in rectangular enclosures in which either a non-scattering or scattering medium is included. The results are compared with the other benchmark approximate solutions. The efficiency and accuracy of the DOM are thus validated.

1. INTRODUCTION

RADIATION either combined with other modes of heat transfer or with combustion phenomena in a multidimensional enclosure such as a combustion chamber, furnace and porous medium has received much attention due to a realization of its importance in the associated application fields. However, since an exact analytical solution to the highly non-linear integro-differential radiative transfer equation (RTE) is nearly impossible to find, an efficient tool to deal with multidimensional radiative heat transfer is in strong demand to analyse various thermal problems.

Although in the past decades a variety of computational schemes have been developed to obtain an approximate solution to RTE, each scheme has demerits as well as merits in its application. Techniques formerly used to attack RTE include the Eddington and Schuster–Schwarzchild approximations [1]. Even if the Monte Carlo [2] and zone [3] methods are called exact numerical solutions, the former consumes an excessively large computational time and the latter is not easily applicable to analysing a radiatively scattering medium. Furthermore, most of the methods previously adopted to solve RTE are incompatible with the finite difference algorithm used in solving the continuity, momentum and energy equations which are involved in various thermal and fluid mechanical problems.

Bayazitoglu and Higenyi [4] and Menguc [5] made it possible to apply the spherical harmonics method, the so-called P_N approximation, to the multidimensional radiative heat transfer problems. Although this development of the mathematical technique used in the P_N approximation rendered it easier to obtain a solution to RTE, it still consumed a lot of computational time and a significant effort was required for rederiving the governing equations and boundary conditions to improve the accuracy of its solution. The finite element method was also employed for the calculation of a coupled conductive and radiative heat transfer problem in two-dimensional rectangular enclosures [6]. However it was found to be not only time consuming, but also difficult to apply to a scattering medium.

Among others the DOM (S_4 method) has recently received increasingly more attention because of its efficient integration with other finite differenced transport equations. This method, conceptually, belongs to a family of flux models, but corrects lack of couplings among the directional intensities present in some of the conventional flux models. In the DOM, the integro-differential RTE is solved only in a fixed number of discrete directions. At first, this method was developed for application to the neutron transport equations by Carlson and Lathrop [7] and, thereafter, it was computationally applied to a very limited number of radiative heat transfer problems. Recently a number of applications to two-dimensional rectangular and hexahedral enclosures [8, 9] and axisymmetric cylindrical geometries [10, 11] have been accomplished by employing the S_4 approximation. It was also applied to a three-dimensional absorbing, emitting and scattering medium by Fiveland [12] and, therein, the stability and accuracy of its solution were discussed as well.

The current study examines the DOM for a coupled conductive and radiative heat transfer in a two-dimensional rectangular enclosure, of which solutions for a non-scattering medium were benchmarked with both the finite element method [6] and the numerical method using a generalized exponential integral function [13]. The results are also compared with those for an anisotropically scattering pure radiation solution obtained by the product-integration method [14]. After validating the accuracy and efficiency of the DOM in this way, it will be applied to the anisotropically scattering radiation–conduction problem,

NOMENCLATURE

a_0	linear anisotropic phase function coefficient
A, B	areas of each control volume face
G	dimensionless intensity
H^*	heat function
I	intensity
k	thermal conductivity
$\mathbf{n}$	unit normal vector
N	conduction to radiation parameter
$\mathbf{q}$	heat flux vector
Q	dimensionless heat flux
$\mathbf{r}$	dimensionless position vector
T	temperature
V	volume of Pth control volume
x, y	coordinates in Cartesian system
X, Y	dimensionless coordinates in Cartesian system.

Greek symbols

α	absorption coefficient
β	extinction coefficient
ε_w	wall emissivity
Θ	dimensionless temperature
μ, ξ	direction cosines
σ	Stefan–Boltzmann constant
σ_0	scattering coefficient
τ_H	optical height
τ_L	optical width
Φ	scattering phase function
ω_0	scattering albedo
Ω, Ω'	outward and inward directions of radiation.

Subscripts and superscripts

m, m'	direction of the discrete ordinates
n, s, e, w	control volume faces surrounding node point P
P	centre of P cell
R	radiative
w	wall value
x, y	directions of each coordinate.

which has not been solved before. In this work the conductive term is discretized using the central difference scheme, and the S_4 approximation is adopted to model the term of divergence of radiative heat flux in the energy equation. Different from the former works, the solutions will be presented using isothermal contours, vectorial plots of conductive, radiative and total heat fluxes, and heat lines for easy understanding of the phenomena involved.

2. ANALYSIS

2.1. *Basic equations*

The physical model and coordinate system are depicted in Fig. 1 in which a rectangular enclosure with the optical width τ_L and height τ_H is considered. The energy conservation equation consisting of both radiative and conductive heat transfers in an infinitesimal control volume can be expressed as follows:

$$k\nabla^2 T - \nabla\cdot\mathbf{q}^R = 0 \tag{1}$$

where the divergence of the radiative heat flux $\mathbf{q}^R$ is given by

$$\nabla\cdot\mathbf{q}^R = 4\alpha\left(\sigma T^4(\mathbf{r}) - \frac{1}{4}\int_{\Omega=4\pi} I(\mathbf{r},\Omega)\,d\Omega\right). \tag{2}$$

The energy equation (1) can then be rewritten as

$$\frac{1}{\tau_L^2}\frac{\partial^2\Theta(\mathbf{r})}{\partial X^2} + \frac{1}{\tau_H^2}\frac{\partial^2\Theta(\mathbf{r})}{\partial Y^2} = \frac{(1-\omega_0)}{N}\left(\Theta^4(\mathbf{r}) - \frac{1}{4}\int_{\Omega=4\pi} G(\mathbf{r},\Omega)\,d\Omega\right) \tag{3}$$

by introducing the following dimensionless variables and parameters:

$$X = \beta x/\tau_L, \quad Y = \beta y/\tau_H, \quad \tau_L = \beta L, \quad \tau_H = \beta H,$$
$$\omega_0 = \sigma_0/\beta, \quad N = k\beta/4\sigma T_1^3, \quad \Theta = T/T_1, \quad G = I/\sigma T_1^4. \tag{4}$$

In the above expressions N is the conduction to radiation parameter and ω_0 the scattering albedo with α, σ_0 and β the absorption, scattering and extinction coefficients of the medium, respectively. T and I are the temperature and radiative intensity.

If the temperature of the left-hand wall (surface 1)

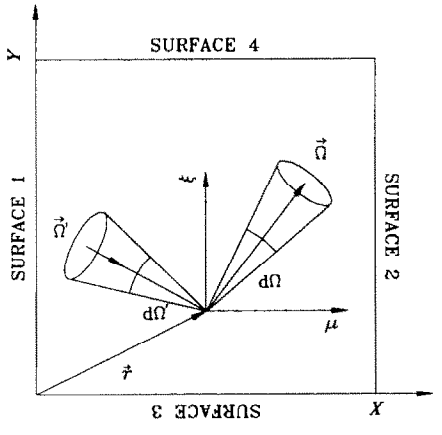

FIG. 1. Schematic of the coordinate system in the rectangular enclosure.

is maintained at T_1 with other walls at T_2, the domain becomes symmetric with respect to $Y = 1/2$. Therefore, only the lower half plane is considered and analysed here. Then the dimensionless boundary conditions for equation (3) become

$$\Theta(0, Y) = 1$$
$$\Theta(1, Y) = \Theta(X, 0) = \Theta_2$$
$$\partial\Theta(X, 1/2)/\partial Y = 0 \tag{5}$$

where $\Theta_2 = T_2/T_1$.

The dimensionless RTE, which represents the balance of energy passing in a specified direction Ω through a small differential volume in an absorbing, emitting and scattering medium, can be written as

$$\frac{\mu}{\tau_L}\frac{\partial G(\mathbf{r},\Omega)}{\partial X} + \frac{\xi}{\tau_H}\frac{\partial G(\mathbf{r},\Omega)}{\partial Y} = -G(\mathbf{r},\Omega) + \frac{(1-\omega_0)}{\pi}\Theta^4(\mathbf{r}) + \frac{\omega_0}{4\pi}\int_{\Omega'=4\pi}\Phi(\Omega'\to\Omega)G'(\mathbf{r},\Omega')\,d\Omega' \tag{6}$$

where the linear anisotropic scattering phase function Φ of energy transfer from the incoming direction Ω' to the outgoing direction Ω can be represented as

$$\Phi(\Omega'\to\Omega) = 1 + a_0(\mu\mu' + \xi\xi') \tag{7}$$

where μ and ξ are the direction cosines of Ω as shown in Fig. 1. Whereas the left-hand side of equation (6) represents the gradient of radiative intensity in the direction of propagation, the terms on the right-hand side illustrate, respectively, the attenuation of intensity due to absorption and out-scattering, and the contribution to the directional intensity due to both the emission from the medium and the in-scattering. The radiative boundary condition for a diffusely reflecting and emitting surface is given by

$$G(\mathbf{r}_w,\Omega) = \frac{\varepsilon_w\Theta^4(\mathbf{r}_w)}{\pi} + \frac{1-\varepsilon_w}{\pi}\int_{\mathbf{n}\cdot\Omega}|\mathbf{n}\cdot\Omega'|G(\mathbf{r}_w,\Omega')\,d\Omega' \tag{8}$$

where ε_w is the surface emissivity, $\mathbf{n}$ the unit normal vector and subscript w denotes the location of the boundary surface. The dimensionless intensity, $G(\mathbf{r}_w,\Omega)$, leaving the boundary surface is composed of two terms; one indicating a contribution to the outgoing intensity due to emission from the surface and the other, the reflection of incoming radiation into the outgoing intensity.

2.2. *Discrete ordinate equations*

In the DOM, equation (6) is solved in a finite number of directions spanning a full range of the total solid angle. A discrete equation for a single subscript m, which is derived from the RTE by substituting a quadrature summed over each ordinate direction into the integral term in equation (6), can be written as

$$\frac{\mu_m}{\tau_L}\frac{\partial G^m}{\partial X} + \frac{\xi_m}{\tau_H}\frac{\partial G^m}{\partial Y} = -G^m + \frac{(1-\omega_0)}{\pi}\Theta^4 + \frac{\omega_0}{4\pi}\sum_{m'}^{M} w_{m'}\{1 + a_0(\mu_m\mu_{m'} + \xi_m\xi_{m'})\}G^{m'}. \tag{9}$$

Table 1. The ordinate direction and weighting factors for the S_4 approximation (one octant only)

Positive direction number	Ordinates μ_m	ξ_m	η_m	Weight w_m
1	0.29588	0.29588	0.90825	0.52360
2	0.90825	0.29588	0.29588	0.52360
3	0.29588	0.90825	0.29588	0.52360

The following radiative boundary conditions are then obtained from equation (8):

$$G^m = \frac{\varepsilon_w}{\pi} + \frac{1-\varepsilon_w}{\pi}\sum_{\mu_{m'}<0} w_{m'}|\mu_{m'}|G^{m'};$$
$$\mu_m > 0 \quad \text{at } X = 0$$
$$G^m = \frac{\varepsilon_w}{\pi}\Theta_2^4 + \frac{1-\varepsilon_w}{\pi}\sum_{\mu_{m'}>0} w_{m'}|\mu_{m'}|G^{m'};$$
$$\mu_m < 0 \quad \text{at } X = 1$$
$$G^m = \frac{\varepsilon_w}{\pi}\Theta_2^4 + \frac{1-\varepsilon_w}{\pi}\sum_{\xi_{m'}<0} w_{m'}|\xi_{m'}|G^{m'};$$
$$\xi_m > 0 \quad \text{at } Y = 0$$
$$G^m = G^{m'} \quad \text{for } \xi_m = -\xi_{m'}; \quad \xi_m < 0 \quad \text{at } Y = 0.5 \tag{10}$$

where m and m' denote the outgoing and incoming directions, respectively.

The choice of ordinate directions Ω_m and quadratic weighting factor w_m is arbitrary, although the symmetry and invariance properties of the physical system are to be preserved. However, a completely symmetric quadrature is to be preferred because of its generality [7]. Generally there are $n(n+2)$ directions for $n = 2, 4, 6, \ldots$. This n is the subscript of the commonly used S_n discrete ordinates scheme. For the present study, 24 discrete directions have been chosen and it is called the S_4 approximation ($n = 4$). But there are only 12 independent directions, because an x–y symmetry plane exists for the normalized intensity G. The ordinate directions and quadratic weighting factors, which are used in this study, are given in Table 1 following the works of Fiveland [12].

2.3. *Definition of heat fluxes and heat lines*

The dimensionless directional heat fluxes, Q_x and Q_y, consist of both conduction and radiation. They are thus defined as follows:

$$Q_x = -\frac{4N}{\tau_L}\frac{\partial\Theta}{\partial X} + \sum_m^M w_m \mu_m G^m$$

$$Q_y = -\frac{4N}{\tau_H}\frac{\partial\Theta}{\partial Y} + \sum_m^M w_m \xi_m G^m \qquad (11)$$

where the first and second terms on the right-hand side are dimensionless conductive and radiative heat fluxes, respectively.

The concept of the heat line was discussed by some researchers like Kimura and Bejan [15] and Aggarwal and Manhapra [16]. The heat function H^* can be derived from the energy conservation equation (1), and is defined as

$$-\frac{\partial H^*}{\partial X} = Q_y, \quad -\frac{\partial H^*}{\partial Y} = Q_x. \qquad (12)$$

As such the net energy flow across the heat lines becomes zero as if no mass flow occurs across the streamline in fluid mechanics. In this study the heat line as well as the isotherm are plotted to describe the heat flow pattern.

2.4. *Numerical method*

By integrating equation (9) over a control volume as shown in Fig. 2, the following equation is obtained:

$$\frac{\mu_m}{\tau_L} A_P (G_e^m - G_w^m) + \frac{\xi_m}{\tau_H} B_P (G_n^m - G_s^m) = -V_P (G_P^m + S) \qquad (13)$$

where

$$A_P = \Delta Y_P, \quad B_P = \Delta X_P, \quad V_P = \Delta Y_P \Delta X_P$$

$$S = \frac{(1-\omega_0)}{\pi}\Theta_P^4 + \frac{\omega_0}{4\pi}\sum_{m'}^M w_{m'}\{1 + a_0(\mu_m \mu_{m'} + \xi_m \xi_{m'})\} G_P^{m'}. \qquad (14)$$

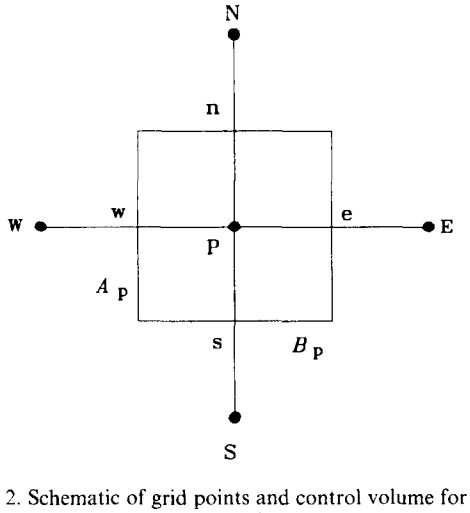

FIG. 2. Schematic of grid points and control volume for the computation.

To relate the facial intensities at the boundary of the control volume to the cell centre intensity, an equally weighted approximation is used

$$2G_c^m = G_{ic}^m + G_{ir}^m. \qquad (15)$$

In the above, i represents the spatial directions, x and y. Subscripts r, e and c denote the reference face or cell centre from which a bundle of intensity originally comes, the end face or cell centre at which the intensity arrives, and the middle point of neighbours, respectively. For a positive set of (μ_m, ξ_m), r, c and e are defined as (w, P, e) with respect to the x-direction and (s, P, n) with respect to the y-direction. Then for the reference facial point, r, c and e become (W, w, P) with respect to the x-direction and (S, s, P) with respect to the y-direction.

Rearranging for the normalized intensity G_P^m by eliminating the facial intensities making use of equation (13) results in

$$G_P^m = \frac{A_P|\mu_m|G_{xr}^m/\tau_L + B_P|\xi_m|G_{yr}^m/\tau_H + V_P S}{A_P|\mu_m|/\tau_L + B_P|\xi_m|/\tau_H + V_P} \qquad (16)$$

where r must be the reference point in the ordinate direction.

A procedure in the numerical calculation starts by assuming that all the boundaries are black and no in-scattering exists. Calculation at each inner point is accomplished for all ordinate directions, starting from the top-right point and marching in the negative x- and y-directions. After one iteration has been completed over a whole domain, the real value of wall emissivity as well as the in-scattering effect is taken into account. In this study the conductive terms in the total energy equation (3) are discretized by the central difference scheme and a uniform grid system is adopted. A typical computing time for each case requires only 3–4 min by using an IBM-AT personal computer powered by one transputer chip for boosting computing speed. The efficiency of the DOM is, therefore, validated here and the accuracy of the solution obtained is discussed in the following section.

3. RESULTS AND DISCUSSIONS

In the present study calculations have been carried out for several cases to investigate the effects of conduction to radiation parameter, N, wall emissivity, ε_w, scattering albedo, ω_0, the parameter a_0 in the linearly anisotropic scattering phase function, Φ, and characteristic optical width τ_L and height τ_H. In all cases the dimensionless cold temperature Θ_2 in conditions (5) is set to 0.5.

Figures 3 and 4 show the temperature and dimensionless total heat flux $Q(\mathbf{Q} = \mathbf{Q}_x + \mathbf{Q}_y)$ along the x-direction at the symmetry line $Y = 0.5$ for various values of N. In addition, therein $\omega_0 = 0$ is assumed, which represents a non-scattering medium in which the radiation is emitted and absorbed only.

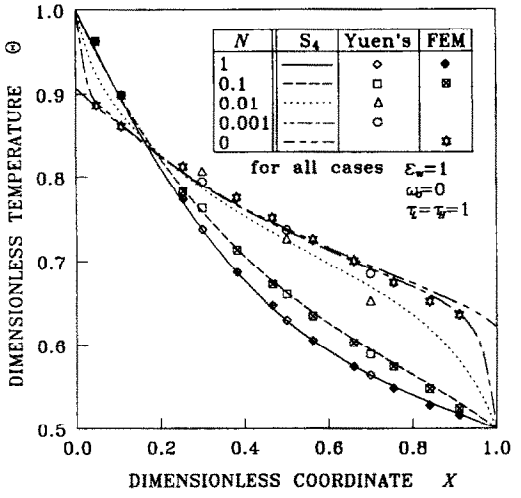

FIG. 3. Dimensionless temperature profiles for various conduction to radiation parameters N along the symmetry line, $Y = 0.5$.

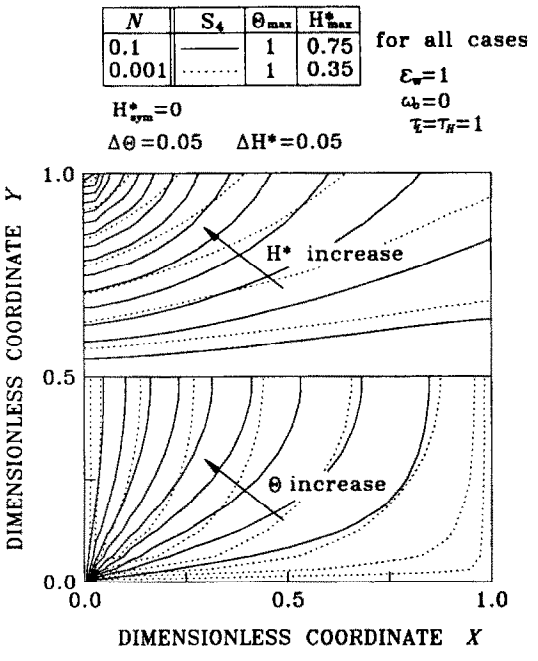

FIG. 5. Isotherms for the lower half region and heat lines for the upper half region with two values of N, 0.1 and 0.001.

As N decreases, radiation plays a more significant role than conduction. Therefore, as N decreases, a steeper temperature gradient is formed at both end walls (surfaces 1 and 2) and the medium temperature inside increases as shown in Fig. 3. This fact is more clearly reflected in Fig. 5 which illustrates the isothermal contours and heat lines depicted, respectively, in the lower and upper half regions of the entire domain for $N = 0.001$ and 1.0. In the figure the non-dimensionalized temperature difference between two neighbouring lines is $\Delta\Theta = 0.05$. For $N = 0.001$ the radiative energy emitted from the wall can penetrate more deeply into the medium and is therein transformed into thermal energy. Therefore, the last isotherm of $\Theta = 0.55$ for $N = 0.001$ is formed very close to the right-hand cold wall (surface 2) compared with that for $N = 0.1$. An excessively steep temperature gradient is established near the lower-left-hand corner where surface 1 intersects surface 3, as can be estimated in Fig. 5, and therein the conduction is predominant over the entire region as will be shown in Figs. 6 and 7.

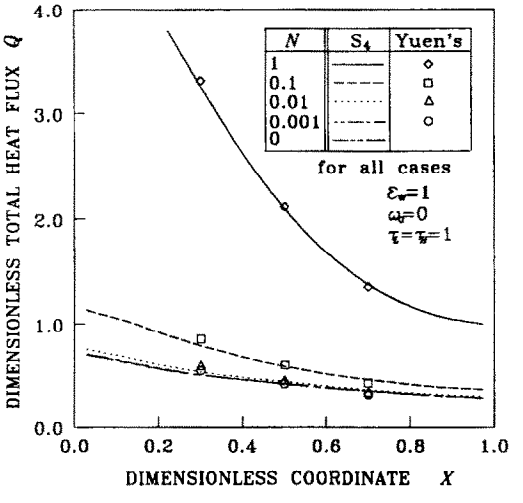

FIG. 4. Variation of total heat flux for various conduction to radiation parameters N along the symmetry line, $Y = 0.5$.

Figure 4 indicates, however, that the total heat flux Q becomes evidently much higher as N increases, i.e. the conduction mode becomes predominant. Therefore, as N decreases the heat blockage effect is observed and the total heat flux is made uniform along the symmetry line $Y = 0.5$. The total heat flow pattern is also shown in Fig. 5 where the value of the heat line is zero on the symmetry line and the difference between two neighbouring heat lines is 0.05. Thus the total heat flow rate is constant between two heat lines and the total heat flux decreases as the gap between two lines increases. Furthermore, it must be noted that the heat transfer cannot take place across the heat lines. Since conduction plays a significant role for $N = 0.1$ compared with $N = 0.001$, heat lines are more bent toward the top cold wall (surface 4) and concentrated near the upper-left-hand corner region where surfaces 1 and 4 are interconnected. This means that the conductive heat loss mainly occurs in that corner. Since for $N = 0.001$ the number of heat lines is small in comparison with $N = 0.1$, the total heat transfer rate from the hot wall (surface 1) is reduced as much for $N = 0.001$.

The total heat flux distribution is more clearly illustrated in Fig. 6, in which the vectorial plots of conductive, radiative and total heat fluxes are separately

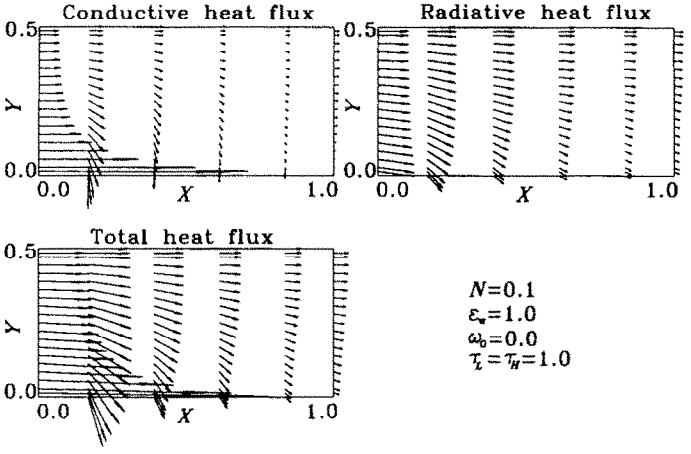

FIG. 6. Vectorial plots of conductive, radiative and total heat fluxes.

presented. Figure 7 shows a variation of the fractional radiative heat flux Q^R/Q along the y-direction at the left-hand hot wall (surface 1) and right-hand cold wall (surface 2). In general the fractional radiative heat flux is seen to decrease as N increases. In the hot wall corner region, the aforementioned extremely large temperature gradient produces a great deal of conductive heat flux as N increases. This can be more evidently noticed in Fig. 6 although not as much of a change in the radiative heat flux occurs in that corner region. For $N = 0.001$, Q^R/Q becomes nearly uniform along both end walls as shown in Fig. 7.

The accuracy of the present solutions is compared with the tabulated results of the generalized exponential integral function by Yuen and Takara [13] as well as the graphic results of the finite element method by Razzaque *et al.* [6]. The temperature profile in Fig. 3 and total heat flux distribution in Fig. 4, which are generated by the present S_4 approximation, are observed to be in very good agreement with the benchmark solutions previously referred to. Therefore, the DOM is considered to be very efficient and accurate.

Figure 8 represents a total heat flux variation with various wall emissivities ε_w at the hot wall (surface 1) for $N = 0.05$ and $\omega_0 = 0$. As the wall emissivity increases, the intensity at the hot wall becomes strong and it further increases the radiative heat flux and the temperature of the medium inside. The temperature gradient in the vicinity of the hot wall is thus reduced and the conductive heat flux therein is reduced by as much. This effect of emissivity is found to be more pronounced for a thicker medium which has a higher optical thickness. In the figure the present solutions obtained by means of the S_4 approximation are shown to be very accurate compared with the marked solutions obtained by FEM [6]. In Fig. 9 the fractional radiative heat flux variation at the symmetry line $Y = 0.5$ and bottom wall (surface 3) is illustrated. In

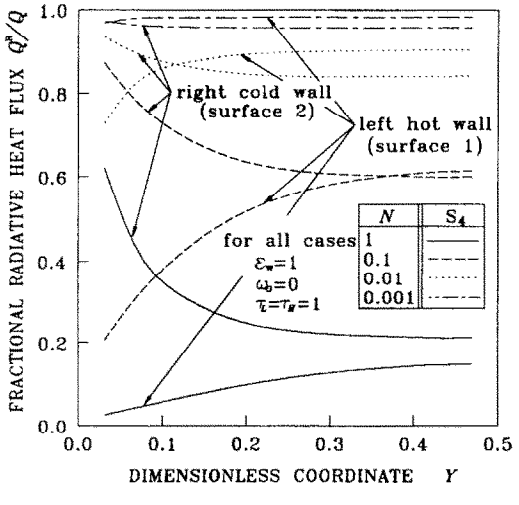

FIG. 7. Variation of fractional radiative heat flux for various conduction to radiation parameters N at the left-hand hot wall, $X = 0$, and at the right-hand cold wall, $X = 1$.

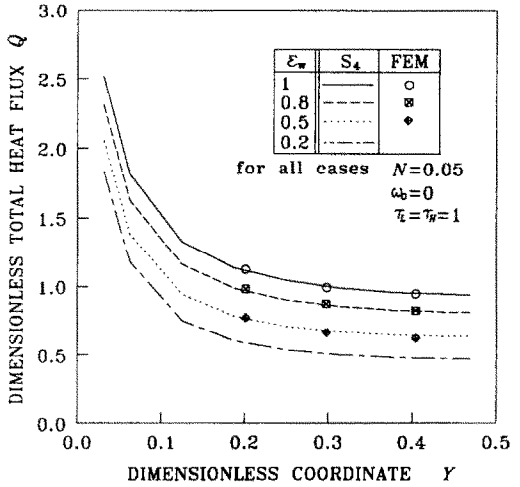

FIG. 8. Variation of total heat flux for various wall emissivities ε_w at the left-hand hot wall, $X = 0$.

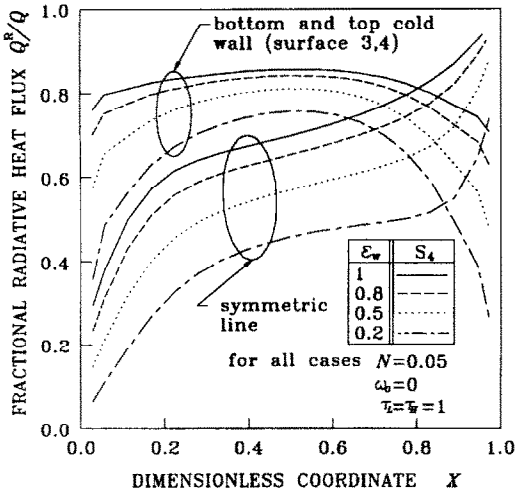

FIG. 9. Variation of fractional radiative heat flux for various wall emissivities ε_w at the symmetry line, $Y = 0.5$, bottom and top walls, $Y = 0, 1$.

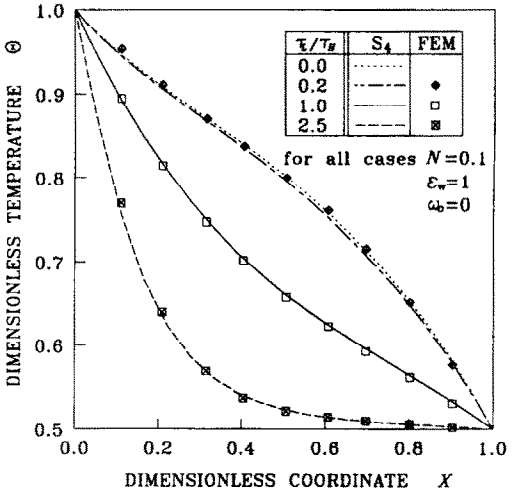

FIG. 11. Dimensionless temperature profiles for various aspect ratios τ_L/τ_H along the symmetry line, $Y = 0.5$.

general as ε_w increases, the radiation becomes dominant owing to the strong intensity emitted from the hot wall (surface 1). Along the bottom or top wall, Q^R/Q is symmetrically distributed with a maximum at its centre. However, on the symmetry line Q^R/Q steadily increases from the hot wall ($X = 0$) to the cold wall ($X = 1$).

Figure 10 shows the effect of albedo ω_0 and parameter a_0 in the linearly anisotropic scattering phase function Φ on the total heat flux at the hot wall for $N = 0$ and 0.01. The values of $a_0 = 1, 0$ and -1 denote forward, isotropic and backward scattering, respectively. As shown in the figure, the total heat flux Q is significantly influenced by the type of scattering. In order to check the accuracy the total heat flux for the limiting case, $N = 0$, which characterizes a purely radiating medium without conduction involved, is compared with the solution obtained by the product-integration method [14]. Note that the total heat flux becomes higher as the parameter $\omega_0 a_0$ increases. The reason is that the strong forward scattering intensifies the amount of radiation in that direction. On the contrary, the backward scattering diminishes the forward radiative intensity. The case for $\omega_0 a_0 = 0$ corresponds to a non-scattering medium in which only absorption and emission take place.

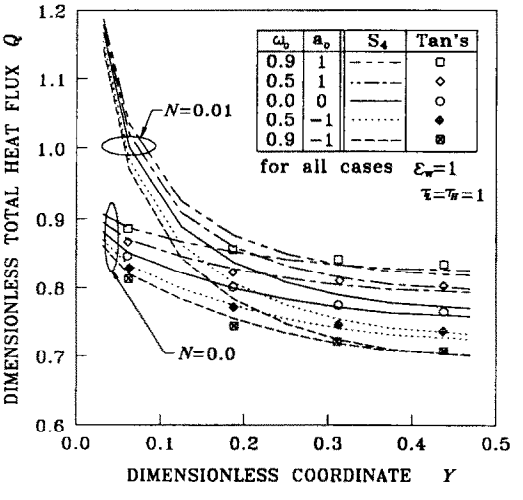

FIG. 10. Variation of total heat flux for various scattering albedos ω_0, and coefficients of linear anisotropic scattering phase function a_0 at the left-hand and hot wall, $X = 0$.

A variation of dimensionless temperature along the symmetry line for different aspect ratios (τ_L/τ_H) with $N = 0.1$, $\varepsilon_w = 1$ and $\omega_0 = 0$ is shown in Fig. 11. The temperature profile for $\tau_L/\tau_H = 0.2$ nearly approaches that for the one-dimensional case, $\tau_L/\tau_H = 0$. It is taken for granted that as τ_L/τ_H increases, the medium temperature very quickly reaches the right-hand cold wall temperature $\Theta_2 = 0.5$.

In Fig. 12, the total heat flux variation for various characteristic optical thicknesses (τ_L or τ_H) of the square enclosure with $N = 0.001$, $\varepsilon_w = 1$ and $\omega_0 = 0$ is plotted along the symmetry line. In the figure, as the characteristic optical thickness (τ_L or τ_H) decreases for fixed $N = 0.001$, the total heat flux increases. Physically the decrease in τ_L or τ_H, with no change of N, means a reduction of the spatial size of the square enclosure because the value of each component, β, k and T_1 in N is fixed in this case. Therefore, Fig. 12 illustrates that as the size of the square enclosure is reduced, the heat loss from the enclosure increases. This can be more clearly shown in the two-dimensional configuration of heat line H^* in Fig. 13 as was done in Fig. 5. As the optical thickness increases, the number of heat lines decreases and thus the total heat loss from the enclosure decreases as well. The comparison of the present results with those obtained by the numerical method using the generalized expon-

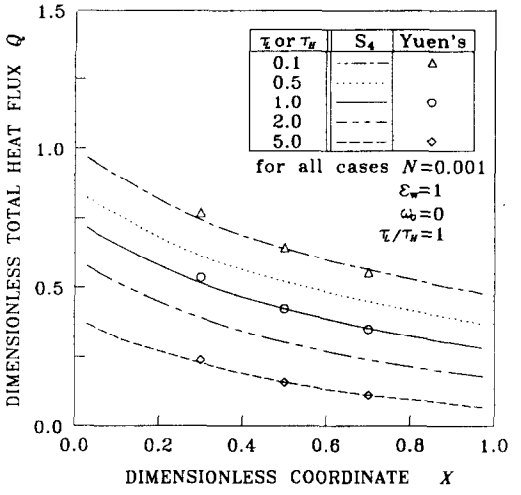

FIG. 12. Variation of the total heat flux for various optical widths or heights (τ_L or τ_H) of the square enclosure ($\tau_L/\tau_H = 1$) along the symmetry line, $Y = 0.5$.

ential integral function [13] shows a good agreement as shown in Fig. 12.

4. CONCLUSIONS

In this study a combined radiative and conductive heat transfer has been investigated in rectangular enclosures. The accuracy and efficiency of DOM (S_4 approximation) were validated by comparing the numerical results for the non-scattering radiation-conduction problem as well as the anisotropically scattering pure radiation problem with other benchmark solutions. It is then applied to the anisotropically scattering radiation-conduction problem to seek new solutions. The results for the temperature distribution and isothermal contours were illustrated. Additionally to easily figure out the involved phenomena, the heat lines and the vectorial plots of the conductive, radiative and total heat fluxes were also introduced and discussed. Conclusively the discrete ordinates method is considered to be highly integrable with other finite differenced transport equations. Furthermore, it was found that only a reasonably short computational time was required to yield quite accurate solutions.

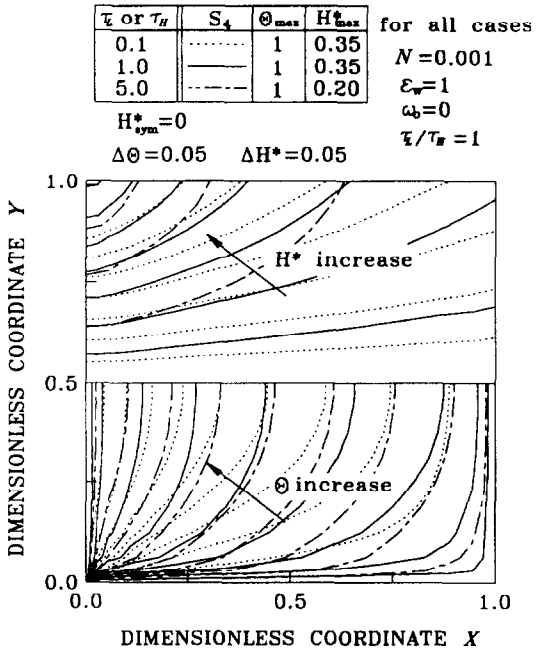

FIG. 13. Isotherms for the lower half region and heat lines for the upper half region with three optical widths or heights (τ_L or τ_H), 0.1, 1.0 and 5.0.

Acknowledgements—The financial assistance by the Objective Research Fund of the Korea Science and Engineering Foundation is gratefully acknowledged.

REFERENCES

1. M. N. Ozisik, *Radiative Transfer*. Wiley, New York (1973).
2. J. R. Howell, Application of Monte-Carlo to heat transfer problem. In *Advances in Heat Transfer* (Edited by T. F. Irvine and J. P. Hartnett), Vol. 5, pp. 1–54. Academic Press, New York (1968).
3. J. J. Noble, The zone method: explicit matrix relations for total exchange areas, *Int. J. Heat Mass Transfer* **18**, 261–269 (1975).
4. Y. Bayazitoglu and J. Higenyi, Higher-order differential equations of radiative transfer: $P-3$ approximation, *AIAA J.* **17**(4), 424–431 (1980).
5. M. P. Menguc, Modeling of radiative heat transfer in multidimensional enclosures using spherical harmonics approximation, Ph.D. Dissertation, Purdue University (1985).
6. M. M. Razzaque, J. R. Howell and D. E. Klein, Coupled radiative and conductive heat transfer in a two-dimensional rectangular enclosure with gray participating media using finite elements, *J. Heat Transfer* **106**, 613–619 (1984).
7. B. G. Carlson and K. D. Lathrop, Transport theory—the method of discrete ordinates. In *Computing Methods in Reactor Physics* (Edited by H. Greenspan, C. N. Kelber and D. Okrent), pp. 165–266. Gordon & Breach, New York (1968).
8. W. A. Fiveland, Discrete ordinates solutions of transport equation for rectangular enclosures, *J. Heat Transfer* **106**, 699–706 (1984).
9. A. S. Jamaluddin and P. J. Smith, Predicting radiative transfer in rectangular enclosures using the discrete ordinates method, *Combust. Sci. Technol.* **59**, 321–340 (1988).
10. J. S. Truelove, Evaluation of a multi-flux model for radiative heat transfer in cylindrical furnaces, HTFS Report No. RS230 (1978).
11. A. S. Jamaluddin and P. J. Smith, Predicting radiative transfer in axisymmetric cylindrical enclosures using the discrete ordinates method, *Combust. Sci. Technol.* **62**, 173–186 (1988).
12. W. A. Fiveland, Three-dimensional radiative heat-transfer solutions by the discrete-ordinates method, *J. Thermophys.* **2**(4), 309–316 (1988).
13. W. W. Yuen and E. E. Takara, Analysis of combined conductive-radiative heat transfer in a two-dimensional

rectangular enclosure with a gray medium, *J. Heat Transfer* **110**, 468–474 (1988).
14. Z. Tan, Radiative heat transfer in multidimensional emitting, absorbing, and anisotropic scattering media—mathematical formulation and numerical method, *J. Heat Transfer* **111**, 141–147 (1989).
15. S. Kimura and A. Bejan, The 'heatline' visualization of convective heat transfer, *J. Heat Transfer* **105**, 916–919 (1983).
16. S. K. Aggarwal and A. Manhapra, Use of heatlines for unsteady buoyancy-driven flow in a cylindrical enclosure, *J. Heat Transfer* **111**, 576–578 (1989).

ANALYSE A L'AIDE DE LA METHODE DES ORDONNEES DISCRETES DE CONDUCTION THERMIQUE DANS UNE CAVITE RECTANGULAIRE BIDIMENSIONNELLE

Résumé—Un outil efficace relatif au transfert radiatif multidimensionnel est recherché pour analyser les problèmes thermiques variés et combinés à d'autres modes de transfert de chaleur ou avec la combustion. On examine la méthode des ordonnées discrètes (DOM) pour le couplage entre rayonnement et combustion thermiques dans des cavités rectangulaires avec ou sans diffusion rayonnante du milieu. Les résultats sont comparés avec d'autres solutions approchées. L'efficacité et la précision de la méthode sont validées.

UNTERSUCHUNG DES KOMBINIERTEN WÄRMEÜBERGANGS DURCH LEITUNG UND STRAHLUNG IN EINEM ZWEIDIMENSIONALEN RECHTECKIGEN HOHLRAUM UNTER VERWENDUNG DES VERFAHRENS DISKRETER ORDINATEN

Zusammenfassung—Es besteht ein dringender Bedarf für ein effizientes Werkzeug zur Behandlung der mehrdimensionalen Wärmeübertragung durch Strahlung, um unterschiedliche thermische Probleme, bei denen andere Arten der Wärmeübertragung oder aber Verbrennungsvorgänge auftreten, zu untersuchen. In der vorliegenden Arbeit wird das Verfahren der diskreten Ordinaten (DOM) für den gekoppelten Wärmeübergang durch Strahlung und Leitung in einem rechteckigen Hohlraum untersucht, in dem sich entweder ein nicht-streuendes oder ein streuendes Medium befindet. Die Ergebnisse werden mit anderen Näherungslösungen verglichen. Die Wirksamkeit und Genauigkeit von DOM wird dabei bestätigt.

АНАЛИЗ ВЗАИМОСВЯЗАННОГО КОНДУКТИВНОГО И ЛУЧИСТОГО ТЕПЛОПЕРЕНОСА В ДВУМЕРНОЙ ПРЯМОУГОЛЬНОЙ С ИСПОЛЬЗОВАНИЕМ МЕТОДА ДИСКРЕТНЫХ КООРДИНАТ

Аннотация—Существует острая необходимость в эффективном методе исследования многомерного лучистого теплопереноса для анализа различных тепловых задач, связанных либо с другими видами теплопереноса, либо с явлениями горения. В настоящей работе методом дискретных координат (DOM) исследуется взаимосвязанный лучистый и кондуктивный теплоперенос в прямоугольных полостях, в которых содержится нерассеивающая или рассеивающая среда. Сравнение полученных результатов с другими приближенными решениями подтверждает эффективность и точность метода дискретных координат.